Vortex Simulation of Spatially Growing Three-Dimensional Mixing Layers

Osamu Inoue*
Tohoku University, Sendai, Japan

Spanwise structures of "nominally" two-dimensional spatially growing turbulent mixing layers are simulated numerically by a three-dimensional vortex method. Small-amplitude three-dimensional disturbances are introduced into an otherwise two-dimensional flowfield. Results show that a large-scale spanwise variation of the flowfield is produced because of amplification of initial disturbances. Pairs of counter rotating streamwise vortices are formed as a result of the stretching and rotation of primary spanwise vortices. The results also suggest that the presence of background disturbances may be essential not only for the formation of streamwise vorticity but also for its sustenance. The results are in good qualitative agreement with the experiments.

Nomenclature

A = amplitude of sinusoidal disturbance
b = mixing-layer thickness, $= y_{0.95} - y_{0.1}$
L = half-width of a duct
L_z = initial length of three-dimensional part of a vortex filament
ℓ = distance between two neighboring vortices upstream of the origin
N = number of vortices in the computational domain
N_{up} = number of vortices upstream of the origin
r = velocity ratio, $= U_2/U_1$
r_v = vorticity ratio, $= |\omega_x|_{max}/|\omega_z|_{max}$
t = time
U = mean velocity in x direction
U_c = convection velocity, $= (U_1 + U_2)/2$
U_1, U_2 = freestream velocities ($U_1 > U_2$)
u,v,w = velocity in x,y,z directions, respectively
x_{max} = downstream distance beyond which vortices are deleted
x_{test} = downstream distance of the test section
x,y,z = streamwise, normal, and spanwise coordinates, respectively
$y_{0.5}$ = normal distance at which $U = U_2 + 0.5\Delta U$
z = complex representation of (x,y), $z = x + iy$
z_0, z_1 = spanwise distance defined in Eq. (9)
Γ_z = circulation of spanwise vortex
ΔU = velocity difference, $= U_1 - U_2$
δt = time step, $= \ell/U_c$
δ_w = vorticity thickness, $= \Delta U/(\partial U/\partial y)_{max}$
ε = numerical core radius
θ = momentum thickness, $= \int (U-U_2)/(U_1-U_2)x[1-(U-U_2)/(U_1-U_2)]\,dy$
λ = wavelength of sinusoidal disturbance
ω_x, ω_z = streamwise and spanwise vorticity components defined in Eq. (10)

Presented as Paper 87-1311 at the AIAA 19th Fluid Dynamics, Plasma Dynamics and Lasers Conference, Honolulu, HI, June 8–10, 1987; received May 19, 1988; revision received Sept. 30, 1988.

*Associate Professor, Institute of Fluid Science. Member AIAA.

Introduction

THE presence of large-scale vortical flow structures in turbulent mixing layers is now well recognized, and the interaction among the vortices is considered to be one of the primary mechanisms in the development of the mixing layers.[1,2] According to recent experiments,[3-7] a "nominally" two-dimensional or "plane" mixing layer contains large-scale, spanwise variation of the flow structure which may be related to the presence of a streamwise vorticity component. Once the streamwise vortices are formed in the flowfield, the primary structure, which originally consists of spanwise vortices only, may be affected. This, in turn, affects the entrainment process.[7] In addition, statistics[8] show that the magnitude of the spanwise component of velocity fluctuation (rms w') is comparable with that of the normal component (rms v'). In this sense, *plane* mixing layers are unquestionably three-dimensional. Thus, three-dimensional approaches to the *plane* mixing layer problem are very desirable from both the experimental and theoretical points of view.

To numerically simulate plane mixing layers, two different approaches are usually taken: direct Navier-Stokes simulation (Eulerian) and vortex simulation (Lagrangian). At present, applications of direct Navier-Stokes simulation are restricted to low Reynolds number flows[9,10] because a large number of grid points are needed to capture small-scale motion in a high Reynolds number flow. The vortex method, on the other hand, has been often applied to simulate mixing layers at a high Reynolds number,[11-15] usually neglecting the viscosity altogether. Presently, most of the applications of the vortex method are based on the assumption of two-dimensional flow, except for the work of Ashurst and Meiburg.[13] Ashurst and Meiburg[13] simulated the initial development of a spatially periodic time-developing three-dimensional mixing layer that was initially perturbed in both the streamwise and spanwise directions. The results showed the formation of streamwise vortices superimposed on the spanwise vortices and suggested that external disturbances may be an origin of three-dimensionality.

This study extends to three dimensions the work done by Inoue and Leonard[14,15] for spatially growing two-dimensional mixing layers. One of the goals of this study was to increase our understanding of the effects of three-dimensionality on the flow features of a plane mixing layer. For this purpose, we used the same flow model and flow parameters (velocity ratio, convection velocity, numerical core radius, etc.) as those used in the study of two-dimensional mixing layers. Small-amplitude three-dimensional disturbances are introduced into an initially two-dimensional mixing layer. Vorticity in the mixing layer is assumed to be represented as a superposition of a

number of vortex filaments. Then each vortex filament is discretized into a number of vortex segments with finite length and with a constant numerical core, and their three-dimensional motion is tracked according to the Biot-Savart law.

Mathematical Formulation and Numerical Procedure

Two-Dimensional Mixing Layers

Before proceeding to the three-dimensional problems, we briefly review the two-dimensional vortex method used by Inoue and Leonard[14,15] because the flow model and the numerical method for two-dimensional mixing layers which we considered in this study are identical to those used by Inoue and Leonard. First, we consider an unbounded flow produced by an infinite row of two-dimensional discrete vortices with the same sign and the same strength moving along the x axis with a constant velocity. Let the circulation of each vortex be denoted by Γ_z, the fixed distance between the two neighboring vortices by ℓ, the constant velocity of the row by U_c, and the upper- and lower-side velocities of the flow far from the x axis by U_1 and U_2, respectively. Then the following relations are satisfied:

$$\Gamma_z = \Delta U \ell, \qquad \Delta U = U_1 - U_2, \qquad U_c = (U_1 + U_2)/2 \tag{1}$$

Let us suppose that at an initial instance $t = 0$ vortices downstream of the origin ($x > 0$) are suddenly removed. At all subsequent times, the vortices upstream of the origin ($x < 0$) are assumed to move along the x axis with the convection velocity U_c. After reaching the origin $x = 0$, each vortex with $x > 0$ is assumed to move under the influence of the potential field induced by individual vortices, including those upstream ($x < 0$) and the convection velocity U_c. Our main interest lies in the motion of the discrete vortices downstream of the origin. To simulate a flow produced in a wind tunnel, the effect of walls that bound the mixing layer at $y = \pm L$ is taken into consideration. In Ref. 14, three simplified treatments of the walls were considered. The difference of the calculated results among the three wall models was slight. In this study, the effect of walls is approximated by two vortex sheets (model C in Ref. 14, see Fig. 1) because the computation time required by this model is about one-third the computation time by the other two models. The vortex sheets are located at $y = \pm 2L$. The prescribed strength of the vortex sheets is such that the total circulation of the flowfield is zero. Strictly speaking, normal velocities on our walls do not vanish. However, it has been confirmed in Ref. 14 that they remain very small. The velocity components u in the x direction and v in the y direction of this two-dimensional flowfield are given by

$$u - iv = U_c + i \sum_{n=1}^{N} \frac{\Gamma_z}{2\pi} \frac{1}{z - z_n} + i \frac{\Gamma_z}{4\pi\ell} \log \frac{z_{\max,u} - z}{z_{\mathrm{up},u} - z} + i \frac{\Gamma_z}{4\pi\ell} \log \frac{z_{\max,\ell} - z}{z_{\mathrm{up},\ell} - z} \tag{2}$$

where $z = x + iy$ and $z_{\max}$ and z_{up} are the downstream and upstream positions of the vortex sheets, respectively. The symbol N denotes the number of discrete vortices in the flowfield, and the subscripts u and ℓ denote the upper and lower vortex sheets, respectively. The second term of the right-hand side of Eq. (2) indicates the contribution of each discrete vortice; the third and fourth terms, respectively, denote the contributions of upper and lower vortex sheets representing the effect of walls. The following core function was used, instead of the second term of the right-hand side of Eq. (2):

$$u = \frac{\Gamma_z}{2\pi} \sum_{n=1}^{N} \frac{y - y_n}{(x - x_n)^2 + (y - y_n)^2 + \varepsilon^2} \tag{3}$$

where ε is the numerical core radius and a similar expression holds for v. The time development of an individual vortex is determined from the relation

$$\frac{dx_n}{dt} = u_n, \qquad \frac{dy_n}{dt} = v_n \tag{4}$$

To save computation time, we assume a test section to be defined as $0 < x < x_{\mathrm{test}}$ in which reliable results are expected, and vortices far downstream ($x \geq x_{\max} >_{st} x$) of the test section are deleted. We also replace the semi-infinite row of vortices upstream of the origin by a finite number (N_{up}) of vortices. The distance between two neighboring vortices upstream of $x = 0$ was prescribed to be $\ell = U_c \delta t$, where δt is the time step. Thus, vortices are shed one by one at every time step at $x = 0$.

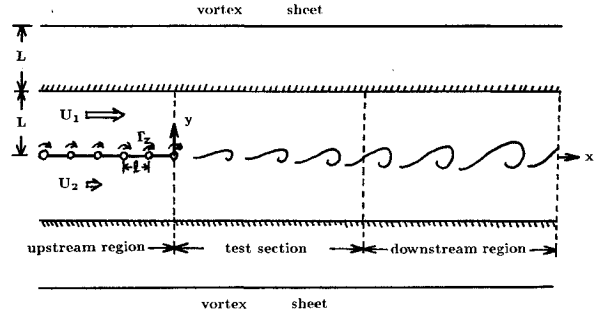

Fig. 1 Schematic of flow model.

Three-Dimensional Mixing Layers

Three-dimensional disturbances are introduced into an initially two-dimensional flowfield. Then each filament of vorticity in the flowfield may undergo three-dimensional displacements, strains, and rotations from its initially two-dimensional state. Following Leonard,[16] each vortex filament is represented as the sum of a two-dimensional unperturbed part and a three-dimensional perturbed part, as shown in Fig. 2a.

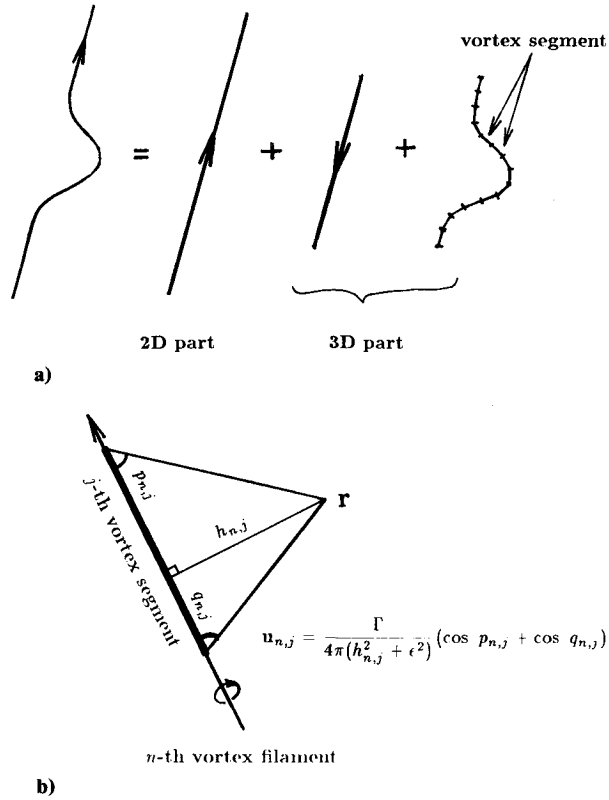

Fig. 2 Method of solution: a) decomposition of vorticity field; b) Biot-Savart law.

The three-dimensional part of a vortex filament consists of a number of vortex segments and one straight vortex filament with finite length which has an opposite sense of rotation to the two-dimensional part. The motion of each vortex segment is analyzed by tracking the motion of each node point according to the Biot-Savart law. The two-dimensional part and the straight vortex filament of the three-dimensional part are assumed to move at a velocity induced to a node point located at a boundary of the three-dimensional part. Accordingly, the velocity field is decomposed as

$$u(r) = U_c + u(r)_{2D} + u(r)_{3D} + u(r)_{sh} \tag{5}$$

where $u = (u,v,w)$ and $r = (x,y,z)$. The second term of the right-hand side of Eq. (5) indicates the contribution of the two-dimensional part of vortex filaments, the third term that of the three-dimensional part, and the fourth term that of the vortex sheets representing the effect of walls. Except for the contribution of the three-dimensional part of the vortex filament, $u(r)_{3D}$, the expressions for each contribution are identical to those described in Eq. (2) for two-dimensional flows. The velocity induced at position r by the jth vortex segment of the nth vortex filament may be expressed, according to the Biot-Savart law, as

$$u_{n,j} = \frac{\Gamma_z}{4\pi(h_{n,j}^2 + \varepsilon^2)} (\cos p_{n,j} + \cos q_{n,j}) \xi_{n,j} \tag{6}$$

where $\epsilon_{n,j} \equiv h_{n,j} e_{n,j}$ and $e_{n,j}$ is the unit vector normal to the plane made by r and the vortex segment. The symbol $h_{n,j}$ is the distance, and $p_{n,j}$ and $q_{n,j}$ are the angles made by the point r and the vortex segment (see Fig. 2b). The three-dimensional part of the velocity field is expressed as

$$u(r)_{3D} = \sum_{n=1}^{N} \sum_{j=1}^{J} u_{n,j} \tag{7}$$

where J is the number of vortex segments of the nth vortex filament. Note that for the special case of a vortex segment with infinite length, i.e., $p_{n,j} = q_{n,j} = 0$, the expression for the induced velocity $u_{n,j}$ by a three-dimensional vortex segment is identical to that for the induced velocity by a two-dimensional discrete vortex, including the finite-core effect [see Eq. (3)].

In this study, vortex filaments upstream of $x = 0$ were assumed to be two-dimensional. At $x = 0$, the three-dimensional part of each vortex filament, whose spanwise length is $2L_z$, was discretized into 50 vortex segments of equal length. With increasing downstream distance, vortex filaments undergo considerable stretching. To maintain spatial resolution, a cubic spline was used to remesh a vortex filament when the length of a vortex segment exceeded twice its initial length. However, in order to save computation time, we stopped adding node points when the total number of node points on the vortex filament increased by a factor of five. Also to save computation time, we assumed that flow is symmetric with respect to the $z = 0$ plane.

Numerical Parameters and Three-Dimensional Initial Disturbances

After a number of preliminary tests, the following parameters were chosen for this study, for both the two- and three-dimensional cases we present:

$$U_c = 3.2, \qquad r(\equiv U_2/U_1) = 0.6, \qquad \delta t = 0.4$$
$$x_{\text{test}} = 250.0, \qquad x_{\max} = 400.0, \qquad L = 50.0$$
$$\varepsilon = 0.6\ell, \qquad N_{\text{up}} = 150 \tag{8}$$

and $L_z = 75.0$ for three-dimensional calculations. The first-order Euler scheme was employed for time integration, because for the case of two-dimensional mixing layers with quite similar flow conditions to the present study, this scheme gave good quantitative agreements with experiments[14,15]. The time step prescribed in this study is four times larger than that used in the two-dimensional mixing layer calculations.[14,15] This larger time step affects the peak values of turbulence intensities but does not affect appreciably the qualitative flow features or the mean velocity profiles.[19] Therefore, only qualitative features are discussed in this paper.

Localized three-dimensional disturbances are provided as follows. Each vortex filament has an initial deformation of a sinusoidal form:

$$x = A\{1 + \cos[2\pi(z - z_0)/\lambda]\}/2$$
$$y = A\{1 + \cos[2\pi(z - z_0)/\lambda]\}/2 \qquad (|z| \leqq z_1 \leqq L_z) \tag{9}$$

We chose $A = 0.15\ell$ and $\lambda = 30$. The choice of wavelength is somewhat arbitrary. It should be mentioned, however, that according to an instability analysis by Pierrehumbert and Widnall,[17] a broad range of wavelengths has approximately the same amplification rates. The amplitude of the deformation is one-fourth of the numerical core radius. For $z_1 < |z| < L_z$, no deformation was given.

This type of disturbance was selected to see the development of *initial* small disturbances in the mixing layer. Jimenez[4] found that the locations of streamwise vortices are often determined by perturbations that originate from wind-tunnel screens or nicks in the nozzle lip. Lasheras et al.[18] found that the position where the formation of three-dimensional structures as first observed changes substantially depending on the location and the intensity of the upstream disturbances. From these experimental observations, the effect of initial disturbances is seen to be important. The choice of *sinusoidal* initial disturbances is based on an idea that any disturbance can be decomposed into its spectral components. For more details, readers are referred to Inoue.[19]

Results and Discussion

Computations were performed for three different values of the wave number of the initial disturbances, i.e., for one-, two-, and five-wave disturbances. However, only the results for the case of five-wave disturbance are presented here, because three-dimensional structures of the flowfield are easier to analyze for this case than for the other two cases, though the cases are similar in many respects.[19] Also, velocity measurements were made only for the five-wave disturbance case.

Flow Visualization

A perspective view of the distribution of vortex filaments in the mixing layer is presented in Fig. 3, and top, side, and rear views are shown in Fig. 4. (Note that a side view is actually an edge view; i.e., we see all the variation of vortex filaments along the span.) In the figures, only the filaments in the region $-60 \leqq z \leqq 60$ of the mixing layer are shown. Vortex filaments downstream of the test section are not shown. In Fig. 3, we look at the flowfield from the higher velocity side. We can see from the perspective view that with increasing downstream distance, the disturbances are amplified and lead to considerable undulation of the vortex filaments along the span and thus the formation of the wavy pattern of the flowfield. Though only three waves are shown in this figure, there are actually two more waves existing on both sides of the figure: the number of the waves of the undulation is the same as the number of the waves of the initial disturbance. Note that the waviness is in phase with the initial disturbance. This result suggests that what occurs is the "translative instability" proposed by Pierrèhumbert and Widnall.[17]

From Figs. 4a and 4b we see that the streamwise vorticity component is produced as a result of the stretching and rotation of spanwise vortices. In our calculations, vortex filaments upstream of $x = 0$ are two-dimensional and thus carry only the spanwise component of vorticity. At $x = 0$, the

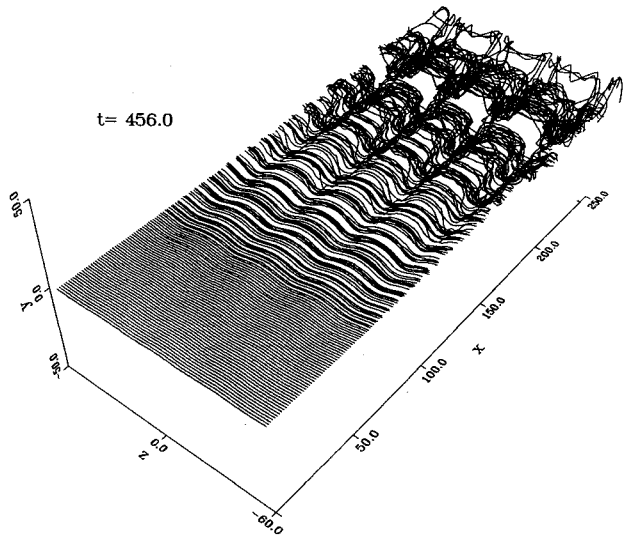

Fig. 3 Perspective view of a three-dimensional mixing layer; $z_0 = 0.0$, $z_1 = 75.0$, 456.0.

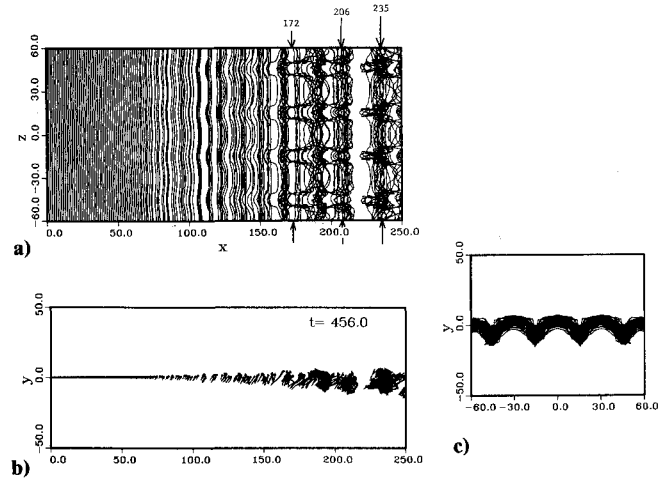

Fig. 4 Three different views of the three-dimensional mixing layer shown in Fig. 3: a) top view; b) side view; c) rear view.

vortex filaments are slightly deformed (i.e., initial small disturbances) so that they have both streamwise and normal components in addition to the original spanwise component of vorticity. The vortex filaments shed at $x = 0$ start to roll up around $x = 75$. During and after the roll up of vortices, the vortex filaments are stretched and rotated. In this process, the spanwise distribution of the streamwise component of vorticity changes from an initial, widely spread, sinusoidal pattern to more a concentrated, square-wave pattern. This concentrated pattern of streamwise vorticity is evident in the braid regions, as seen in the region $150 < x < 200$ in Fig. 4a. Note that the streamwise component of vorticity produced by the stretching and rotation of spanwise vorticity always shows pairs of counter-rotating vortices, which are considered to be characteristic of three-dimensional mixing layers.[7,20] Figure 4a and also our movie picture (not shown here) indicate that these pairs of counter-rotating vortices are formed at fixed spanwise locations. As noted before, however, the undulation of vortices is in phase with the initial disturbances: changes in the initial disturbances may lead to changes in the wavy pattern of the flowfield. Therefore, for a different flow condition, streamwise vortices may be formed at different, but fixed, spanwise locations. This notion is consistent with the observation by Bernal and Roshko[7] in which the spanwise positions of streamwise streaks were fixed for a given flow condition but changes in the upstream screens produced changes in the spanwise positions of the streaks. The undulation of vortices along the span seen in Figs. 3 and 4 is similar to the "corrugated" cores of Jimenez[4] and the "wiggles" observed by Breidenthal.[3] Wavy patterns similar to those shown in Figs. 3 and 4 have also been observed by Jimenez et al.,[6] where three-dimensional patterns of a plane mixing layer were demonstrated by using digital image processing.

From Fig. 4a it may be also interesting to see an asymmetric spacing of counter-rotating streamwise vortices, which is often observed in experiments.[21] Ashurst and Meiburg[13] also observed an asymmetric spacing of counter-rotating streamwise vortices in their time-developing mixing layer. They imposed two opposite signs of vorticity on the flowfield in order to account for the effect of the weaker boundary layer developed on the splitter plate. With one sign of vorticity, they did not see the asymmetry. Thus, Ashurst and Meiburg concluded that both boundary layers emanating from the splitter plate should be included in a mixing-layer simulation in order to see the asymmetric spacing of streamwise vortices. In the present calculation, only one sign of vorticity is imposed and we see the asymmetry. Note that in this calculation initial disturbances are prescribed such that vortex filaments are deformed only in the positive y region [Eq. (9)]. (Ashurst and Meiburg gave symmetric initial disturbances with respect to the $y = 0$ plane for their mixing layer with one sign of vorticity.) Together with the results of Ashurst and Meiburg, it seems that the asymmetric distribution of vorticity with respect to the $y = 0$ plane may cause the asymmetric spacing of counterrotating streamwise vortices in the spanwise direction.

In order to confirm the existence of a streamwise vorticity component, we measured the instantaneous velocities in the (y,z) plane at three different x stations indicated by the arrows in Fig. 4a. The first station ($x = 172$) is in a braid region. The second ($x = 206$) is in a vortex core region. The third ($x = 235$) is in another vortex core region in which vortex pairing is in progress. Velocities were measured at 4961 grid points (41 in y, 121 in z) covering the regions $-20 \leqq y \leqq 20$ and $-60 \leqq z \leqq 60$. The results are plotted in Fig. 5 as velocity vectors. Figure 5a shows clearly that pairs of counter-rotating streamwise vortices exist in the braid region.

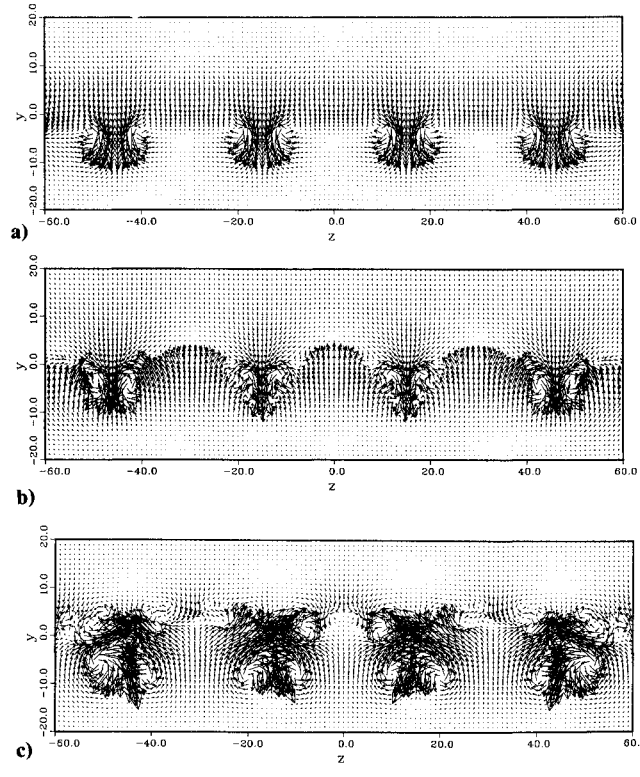

Fig. 5 Plots of velocity vectors in (y,z) plane at three different z stations shown in Fig. 4: a) 172; b) 206; c) 235.

At first glance, it appears from Fig. 5b that pairs of counter-rotating streamwise vortices exist even in the vortex core. This is not the case. A rear view of the vortex core that consists of the vortex filaments in the region $200 \leqq x \leqq 215$ is presented in Fig. 6. As seen from Fig. 6, the vortex core itself is deformed, and this deformed core is inclined to the flow direction; i.e., the streamwise vorticity in this region is produced primarily by the inclination of the deformed vortex core to the streamwise direction. Figure 5c shows that during a vortex pairing process, an additional pair of counter-rotating streamwise vortices appears at each of the four spanwise locations where only one pair of streamwise vortices is seen in Fig. 5b. In Fig. 5c, pairs of streamwise vortices on the higher-speed side have the opposite sense of rotation to those on the lower-speed side. One possible mechanism for their presence is presented as a simplified sketch of the flow configuration in Fig. 7a. In the pairing process, two vortex cores rotate around each other to merge into a larger vortex core, but they are out of phase. Shown in Fig. 8 are velocity vectors in a vortex pairing process at a different time, $t = 760.0$. Again we can see two pairs of streamwise vortices, but in this case these pairs have the same sense of rotation. One possible mechanism for this case is shown in Fig. 7b.

Vorticity Measurement

Instantaneous velocities calculated at a number of grid points in (y,z) planes at three different x stations previously mentioned were used to calculate the streamwise vorticity ω_x. The streamwise and spanwise vorticity components are defined as

$$\omega_x = \frac{\partial v}{\partial z} - \frac{\partial w}{\partial y}, \qquad \omega_z = \frac{\partial u}{\partial y} - \frac{\partial v}{\partial x} \tag{10}$$

A central difference expression was used to evaluate ω_x. The mesh sizes, $\Delta y = \Delta z = 1.0$, are one-third of the initial length of a vortex segment. Similarly, instantaneous velocities at a number of grid points in (x,y) planes at several spanwise locations were also calculated. The number of grid points in the (x,y) planes was 10,291 (251 in x, 41 in y), and the measured region is $0 \leqq x \leqq 250$ and $-20 \leqq y \leqq 20$ ($\Delta x = \Delta y = 1.0$). The five spanwise locations are the plane of symmetry ($z = 0.0$), the point where the initial disturbance has a minimum ($z = -15.0$), and inflection point ($z = -22.5$), a point of maximum ($z = -30.0$), and another inflection point ($z = -37.5$). The spanwise vorticity ω_z at each grid point in the (x,y) plane was calculated in the same way as ω_x. From these measurements of vorticity, we can estimate roughly the vorticity ratio, $r_v \equiv |\omega_x|_{\max}/|\omega_z|_{\max}$, at different streamwise stations. The maximum streamwise vorticity $|\omega_x|_{\max}$ was determined by taking the absolute peak value of ω_x measured at the centers of streamwise vorticity. The maximum spanwise vorticity $|\omega_z|_{\max}$ was determined by the peak value of spanwise vorticity calculated at the five spanwise locations previously described. However, the spanwise vorticity in a braid region is very weak. An average of peak values of ω_z in the two closest cores to the braid was used to evaluate the vorticity ratio in the braid. The results are presented in Table 1, where vorticity components are normalized by the maximum value of the mean shear, $(\partial U/\partial y)_{\max}$, at the station. In Table 1, the results for three different times, $t = 544.0$, 652.0, and 760.0, are also presented. As seen from Table 1, the streamwise vorticity is about two to four times stronger than $(\partial U/\partial y)_{\max}$ at the station and almost the same as the value of spanwise vorticity. From Table 1, we notice that the vorticity ratio in a braid region is sometimes much weaker than that in a core region, as is evident for the case of $t = 652.0$. This result suggests that the streamwise vorticity produced by inclination of the deformed cores to the flow direction (Fig. 6) is significant.

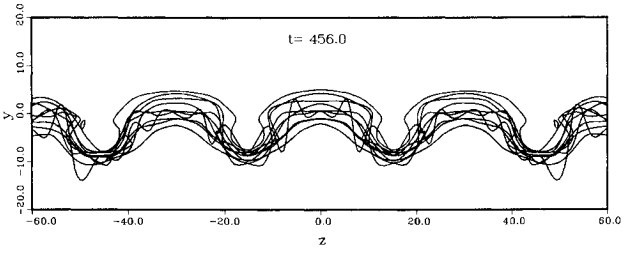

Fig. 6 Plot of vortex filaments that make up the vortex Core around 206.

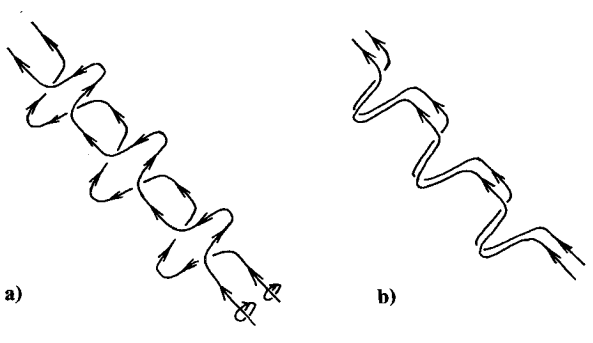

Fig. 7 A sketch of flow configurations during vortex pairing process. Each line in this figure indicates a vortex Core: a) out of phase; b) in phase.

A Model for Three-Dimensional Structures

A simplified model for three-dimensional structures in the mixing layer which is constructed from the *calculated* results is presented in Fig. 9. The characteristic features of the model are the deformation of primarily spanwise vortex cores and the formation of streamwise vortices at fixed spanwise locations. This model is consistent with the models proposed from *experimental* observations by Bernal and Roshko,[7] Jimenez,[4] and Hussain,[5] respectively, and differs only in the omission or inclusion of certain features.[19]

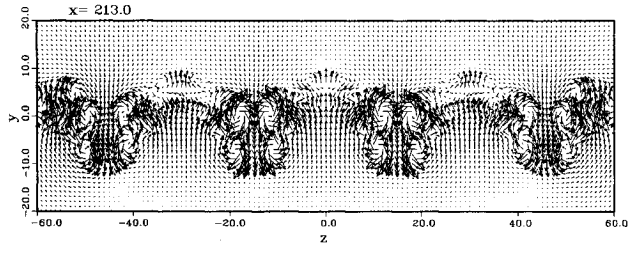

Fig. 8 Plot of velocity vectors in a vortex pairing process at 760.0

Table 1 Vorticity ratio r_v (streamwise to spanwise)

Time	Streamwise station, x	$\lvert\omega_x\rvert_{\max}$	$\lvert\omega_z\rvert_{\max}$	r_v	Region
	172.0	2.18	3.03	0.72	Braid
456.0	206.0	3.06	3.09	0.99	Core
	235.0	4.22	4.14	1.02	Core
	194.0	2.92	3.09	0.95	Core
	203.0	2.38	3.45	0.69	Braid
544.0	211.0	3.54	3.79	0.94	Core
	225.0	4.20	3.05	1.37	Core
	189.0	3.00	5.02	0.60	Core
	198.0	1.36	4.54	0.30	Braid
652.0	205.5	4.69	3.92	1.20	Core
	212.0	2.74	4.02	0.68	Braid
	222.0	6.01	4.17	1.44	Core
	200.0	3.53	3.21	1.10	Core
760.0	206.0	3.54	3.33	1.06	Braid
	213.0	3.41	3.47	0.98	Core

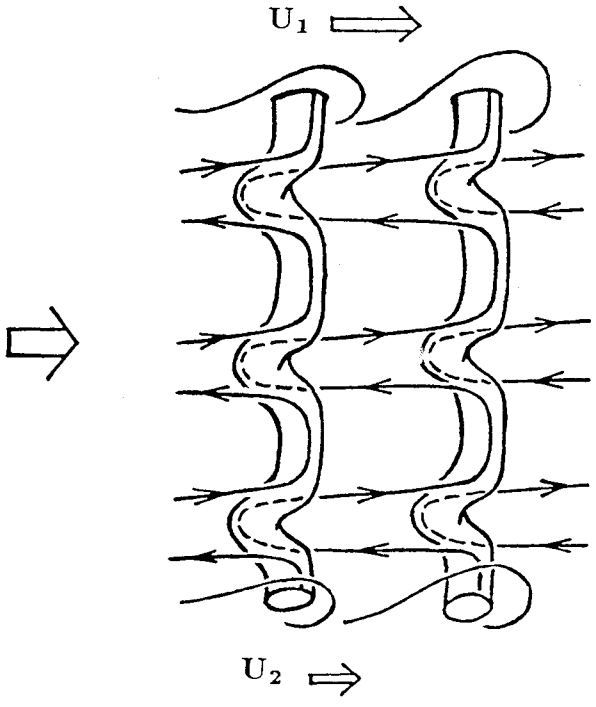

Fig. 9 A simplified model for three-dimensional mixing layers.

Role of Initial Disturbances

As mentioned in the Introduction, three-dimensionality always exists in actual *plane* mixing layers. Why and how does this three-dimensional motion appear? Our calculated results show that once small disturbances are introduced into mixing layers, they are amplified to form streamwise vorticity, and that three-dimensionality exists as long as we keep providing disturbances. Therefore, external disturbances such as nicks in a nozzle lip,[4] a small nonuniformity of a screen in the wind tunnel,[4,7] or surface roughness on a splitter plate[18,22] can be an origin of three-dimensionality. What happens if we stop providing disturbances? Are there any internal mechanisms that sustain three-dimensional motions in a mixing layer? If there are such mechanisms, external disturbances only play the role of a trigger in producing three-dimensional motions. If there is not such a mechanism, the presence of external disturbances is critical not only for the formation of a streamwise vorticity component but also for its sustenance. In order to examine these possibilities numerically, we stopped providing disturbances after a three-dimensional state of a mixing layer had been achieved; i.e., at $t = 340.0$. Figure 10 shows the mixing layer at $t = 448.0$. Three-dimensional motions have decayed, and a two-dimensional state is revived with increasing time t. This suggests that the presence of external (or upstream) disturbances may be critical for the formation of streamwise vorticity in a plane mixing layer.

Growth Rates

Velocity measurements were made across the layer (41 points for $-20 \leqq y \leqq 20$) at four spanwise locations at each of five streamwise stations ($140 \leqq x \leqq 220$). The spanwise stations are $z = -7.5$, -15.0, -22.5, and -30.0, corresponding to points of inflection, minimum, inflection, and maximum, respectively, of the initial disturbance. The mean flow quantities were obtained by averaging instantaneous values over the period $374.0 \leqq t \leqq 806.0$. This gives 1080 samples. It has been confirmed that, at least for two-dimensional flows, this averaging time is sufficient to obtain accurate values of characteristic thicknesses of a mixing layer.[19]

The three characteristic thicknesses and the locus of $y_{0.5}$, which are measured at the four different spanwise locations, are presented in Fig. 11. In the figure $y_{0.5}$ is the center of the mixing layer. The dashed line is the average of the values at

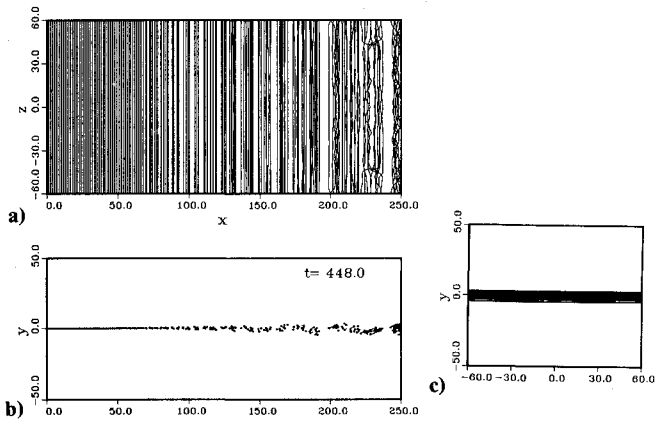

Fig. 10 Three-dimensional mixing layer sufficiently after introduction of initial disturbances is stopped, $t = 448.0$: a) top view; b) side view; c) rear view.

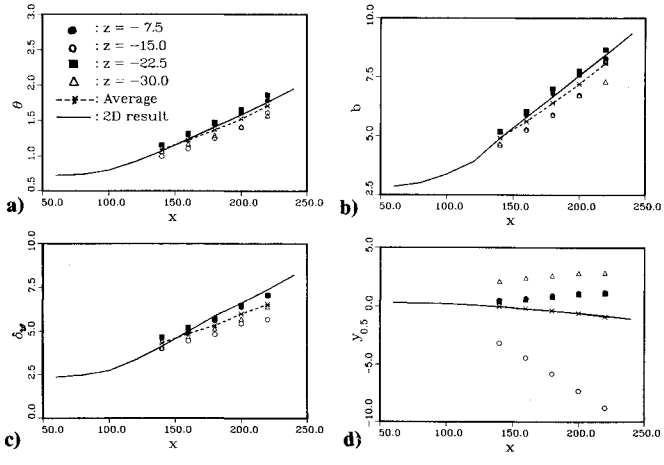

Fig. 11 Various thicknesses and locus of $y_{0.5}$ for a three-dimensional mixing layer: a) θ; b) b; c) δ_w; d) $y_{0.5}$. —— : two-dimensional results; – – – – : average values over the four spanwise locations.

the four spanwise locations. The results for the two-dimensional mixing layer are shown by the solid lines. All the averaged values (dashed lines) of each thickness show, respectively, linear growth of the mixing layer. The plot of $y_{0.5}$ shows that the center of the mixing layer moves toward the lower-speed side at $z = -15.0$ while it moves toward the higher-speed side at the other three z stations. As seen in Fig. 5, streamwise vortices are formed at fixed spanwise locations around $z = -11.0$, -19.0, -41.0, and -49.0 in the region of $z \leqq 0$. Thus, among the four spanwise locations where velocity measurements were made, only at $z = -15.0$ (point of minimum) is downward velocity induced by the streamwise vortices, indicating that fluid particles in the higher-speed region are entrained into the mixing layer at this location. On the other hand, at the other three z locations, upward velocity is induced by the streamwise vortices. As a result, fluid particles in the lower-speed region are entrained at these locations and the center of the mixing layer moves toward the higher-speed side. This result is consistent with the experimental observation by Bernal and Roshko[7] using a concentration measurement, where preferential entrainment of nonturbulent fluid from one side of the layer at different spanwise locations was found. Interestingly, the averaged positions of $y_{0.5}$ (the dashed line) almost coincide with the results for the two-dimensional mixing layer (the solid line), and indicate that as a whole, the three-dimensional mixing layer moves toward the lower-speed side. The asymmetric entrainment, which favors the higher-speed fluid particles, was observed by Konrad,[21] Oster and Wygnanski,[8] and others and numerically confirmed by Grin-

stein, Oran and Boris,[23] and Inoue and Leonard.[14,15] Dimotakis[24] explains the asymmetric entrainment from the two-dimensional point of view.

Summary and Concluding Remarks

Spanwise structures of "nominally" two-dimensional spatially growing turbulent mixing layers are simualted numerically by a three-dimensional vortex method. Primary results are as follows: 1) A large-scale spanwise variation of the flowfield is produced because of amplification of initial disturbances; 2) pairs of counter-rotating streamwise vortices are formed as a result of stretching and rotation of primary spanwise vortices; 3) the streamwise vortices are formed at a fixed spanwise location that depends on initial disturbances; 4) the calculated magnitude of streamwise vorticity is close to that of the spanwise vorticity; 5) deformation of vortex cores and their inclination to the flow direction are important in the formation of streamwise vorticity in the core region; 6) the presence of background disturbances may be essential not only for the formation of streamwise vorticity but also for its sustenance; and 7) depending on the location of streamwise vortices, nonturbulent fluid particles from one side of the mixing layer are preferentially entrained at different spanwise locations.

Acknowledgments

The author expresses his sincere thanks to Prof. A. Leonard at the California Institute of Technology, and to Drs. N. N. Mansour, R. D. Mehta, K. Shariff, and P. R. Spalart at NASA Ames Research Center for valuable advice and fruitful discussions. Thanks are also given to Profs. P. E. Dimotakis and J. E. Broadwell at CalTech for their useful advice. The major part of this work was done at NASA Ames Research Center, which the author thanks. This work was supported by National Research Council Scholarship.

References

[1]Roshko, A., "Structure of Turbulent Shear Flow: A New Look," *AIAA Journal*, Vol. 14, 1976, pp. 1349–1357.

[2]Ho, C. M. and Huerre, P., "Perturbed Free Shear Layers," *Annual Review of Fluid Mechanics*, Vol. 16, 1984, pp. 365–424.

[3]Breidenthal, R., "Structure in Turbulent Mixing Layers and Wakes Using a Chemical Reaction," *Journal of Fluid Mechanics*, Vol. 109, 1981, pp. 1–24.

[4]Jimenez, J., "A Spanwise Structure in the Plane Shear Layer," *Journal of Fluid Mechanics*, Vol. 132, 1983, pp. 319–336.

[5]Hussain, A. K. M. F., "Coherent Structures and Incoherent Turbulence," *Turbulence and Choatic Phenomena in Fluids*, edited by T. Tatsumi, North-Holland, Kyoto 1983, pp. 453–460.

[6]Jimenez, J., Cogollos, M., and Bernal, L. P., "A Perspective View of the Plane Mixing Layer," *Journal of Fluid Mechanics*, Vol. 152, 1985, pp. 125–143.

[7]Bernal, L. P. and Roshko, A., "Streamwise Vortex Structure in Plane Mixing Layers," *Journal of Fluid Mechanics*, Vol. 170, 1986, pp. 499–525.

[8]Oster, D. and Wygnanski, I., "The Forced Mixing Layer Between Parallel Streams," *Journal of Fluid Mechanics*, Vol. 123, 1982, pp. 91–130.

[9]Metcalfe, R., Menon, S., and Hussain, A. K. M. F., "Physics of the Mixing Layer: Direct Numerical Simulations and Experiments," AIAA Paper 87-1249, 1987.

[10]Grinstein, F. F., Oran, E. S., and Hussain, A. K. M. F., "Three-Dimensional Numerical Simulation of a Compressible, Spatially Evolving Mixing Layer," AIAA Paper 88-0042, Jan. 1988.

[11]Ashurst, W. T., "Numerical Simulation of Turbulent Mixing Layers via Vortex Dynamics," *Turbulent Shear Flows*, edited by Durst, Springer-Verlag, New York, 1979, pp. 402–413.

[12]Ghoniem, A. F. and Ng, K. K., "Effect of Harmonic Modulation on Rates of Entrainment in a Confined Shear Layer," AIAA Paper 86-0056, Jan. 1986.

[13]Ashurst, W. T. and Meiburg, E., "Three-Dimensional Shear Layers via Vortex Dynamics," Sandia National Laboratories, Livermore, CA, SAND 85-8777, 1985.

[14]Inoue, O. and Leonard, A., "Vortex Simulation of Forced Mixing Layers," NASA TM 88235, 1986.

[15]Inoue, O. and Leonard, A., "Vortex Simulation of Forced/Unforced Mixing Layers," *AIAA Journal*, Vol. 25, Nov. 1987, pp. 1417–1418. See also AIAA Paper 87-0288, 1987.

[16]Leonard, A., "Computing Three-Dimensional Incompressible Flows with Vortex Elements," *Annual Review of Fluid Mechanics*, Vol. 17, 1985, pp. 523–599.

[17]Pierrehumbert, R. T. and Widnall, S. E., "The Two- and Three-Dimensional Instabilities of a Spatially Periodic Shear Layer," *Journal of Fluid Mechanics*, Vol. 114, 1982, pp. 59–82.

[18]Lasheras, J. C., Cho, J. S., and Maxworthy, T., "On the Origin and Evolution of Steamwise Vortical Structures in a Plane Free Shear Layer," *Journal of Fluid Mechanics*, Vol. 172, 1986, pp. 231–258.

[19]Inoue, O., "Vortex Simulation of Three-Dimensional Turbulent Mixing Layers," AIAA Paper 87-1311, 1987.

[20]Roshko, A., "The Plane Mixing Layer, Flow Visualization Results and Three Dimensional Effects," *Lecture Notes in Physics*, Springer-Verlag, Vol. 136, 1980, pp. 208–217.

[21]Konrad, J. H., "An Experimental Investigation of Mixing in Two-Dimensional Turbulent Shear Flows with Applications to Diffusion-Limited Reactions," Project SQUID, Technical Report CIT-8-PU, 1976.

[22]Ho, C. M., "Mixing Processes in Free Shear Layers," AIAA Paper 86-0234, 1986.

[23]Grinstein, F. F., Oran, E. S., and Boris, J. P., "Numerical Simulation of Asymmetric Mixing in Planar Shear Flows," *Journal of Fluid Mechanics*, Vol. 165, 1986, pp. 201–220.

[24]Dimotakis, P. E., "Two-Dimensional Shear-Layer Entrainment," *AIAA Journal*, Vol. 24, pp. 1791–1796.